

# Field Test Results from the Sandia SMART Rotor

Jonathan C. Berg<sup>\*</sup> and Matthew F. Barone<sup>†</sup> and Brian R. Resor<sup>‡</sup>  
*Sandia National Laboratories<sup>\*\*</sup>, Albuquerque, NM, 87185-1124*

**Sandia National Laboratories has concluded field testing of its wind turbine rotor equipped with trailing-edge flaps. The blade design, fabrication, and integration which have been described in previous papers are briefly reviewed and then a portion of the data is presented and analyzed. Time delays observed in the time-averaged response to stepwise flap motions are consistent with the expected time scales of the structural and aerodynamic phenomena involved. Control authority of the flaps is clearly seen in the blade strain data and in hub-mounted video of the blade tip movement.**

## I. Introduction

ONE means of reducing the cost of energy for wind turbines is through reduction of component weight. One approach for accomplishing this is to reduce loads on the machine through active or passive blade load control. In an active load control approach, aerodynamic loads on the blades are reduced through the use of flow control actuators, such as trailing edge flaps, a deformable trailing edge, or small trailing edge tabs. These Active Aerodynamic Load Control (AALC) devices are combined with sensors for measuring aerodynamic loads, structural loads, and/or dynamic structural motion to create a closed-loop control system.

A recent review of concepts and feasibility and an inventory of design options for such systems have been performed by Barlas and van Kuik at Delft University of Technology (TU Delft)<sup>1</sup>. Active load control utilizing trailing edge flaps or deformable trailing edge geometries is receiving significant attention because of the direct lift control capability of such devices and recent advances in smart material actuator technology. Researchers at TU Delft<sup>2-3</sup>, Risø/Danish Technical University Laboratory for Sustainable Energy (Risø/DTU)<sup>4-10</sup> and Sandia National Laboratories (SNL)<sup>11-17</sup> have been very active in this area over the past few years.

Sandia's involvement with active load control can be traced back to collaborations with C.P. van Dam and R. Chow on the microtab device concept<sup>18</sup> and also the internal efforts of D. Berg, Zayas, and Lobitz to identify the controls, sensors, and actuators needed to implement these or similar devices<sup>19</sup>. Since that time, work has steadily progressed to improve simulation capabilities and evaluate the potential benefits of active aerodynamic devices (AAD) on wind turbine performance. This work established hypothetical approaches for integrating active devices into the wind turbine structure and controllers, but the research area has needed the validation and additional insight that a field test would provide. In 2010, Sandia initiated a three-year project to design, build, and test a rotor with integrated sensors and conventional hinged trailing-edge flaps (or ailerons, depending on preferred terminology). Although previous work had investigated various active devices including microtabs and variable (morphing) trailing edge geometry, the choice of conventional hinged flaps was motivated by an expectation of good aerodynamic control authority and relative simplicity of integration. The primary objective driving the project was to evaluate the aero-servo-elastic simulation tools rather than develop the most efficient AAD design and implementation.

## II. Blade Design & Fabrication

The design, fabrication, and integration of the SNL flapped rotor was described in previous AIAA papers<sup>20-21</sup>. The main content of those papers regarding the blade design is now reviewed briefly.

---

<sup>\*</sup> Wind Energy Technology Department, Mail Stop 1124, AIAA Senior Member

<sup>†</sup> Aerosciences Department, Mail Stop 0825, AIAA Senior Member

<sup>‡</sup> Wind Energy Technology Department, Mail Stop 1124, AIAA Senior Member

<sup>\*\*</sup> Sandia National Laboratories is a multi-program laboratory managed and operated by Sandia Corporation, a wholly owned subsidiary of Lockheed Martin Corporation, for the U.S. Department of Energy's National Nuclear Security Administration under contract DE-AC04-94AL85000.

Leveraging the existing SNL CX-100 blade design, a plan was developed to fabricate a set of blades using the standard build process used on previous CX-100 builds and then modify the outboard trailing edge to accept a set of three active flap modules. Because a significant portion of the blade would be removed, layers of double-bias carbon replaced glass fiber in this region to compensate for the loss of stiffness. After TPI Composites completed fabrication of the skins for these 9-meter blades, they were instrumented on the internal blade surfaces with accelerometers, fiber optic strain, fiber optic temperature, and metal foil strain gages. The approximate locations of these sensors are shown in Figure 1. The blades were then closed and finished at TPI and then shipped to Sandia for subsequent modification of the trailing edge. The active flaps were designed to be 20% of chord in width and roughly 20% of blade span in length and have a range-of-motion of  $\pm 20$  degrees. To integrate the flap modules, a trailing-edge blade section was removed starting at span 7.029m and ending at 8.857m. The width of the cutout, measured from the trailing edge, was 40% at the inboard end and then expanded linearly to 50% of chord at the outboard end. This cutout did not extend to the tip of the blade – the outer 14.3cm (one tip chord length) of the trailing edge was left intact to minimize the impact of the blade tip vortex on the performance of the flaps. A custom-built spar was fabricated for each blade and installed within the cutout to regain the blade structure needed for strength and to provide a flat mounting surface for the modules.

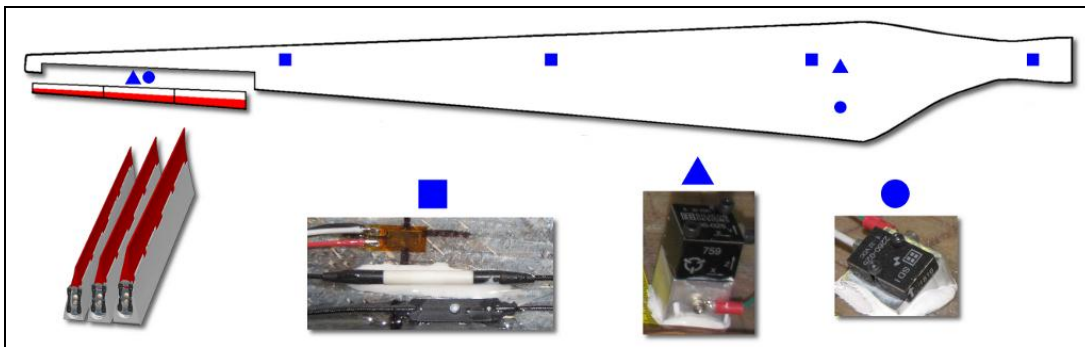


**Figure 1. Schematic of internal sensor locations. (Square) foil strain, fiber-optic temperature, and fiber-optic strain. (Triangle) tri-axial accelerometer. (Circle) uni-axial accelerometer.**

### III. Test Turbine

The rotor was installed on the SNL turbine (Figure 2) located on the USDA-ARS site in Bushland, Texas, USA. The test turbine is a three-bladed, constant speed, fixed-pitch, upwind Micon 65/13 turbine with modifications to the brakes, gearbox, generator, and blades. The generator is rated at 115 kW and operates at 1200 rpm while the rotor turns at a nominal 55 rpm (the standard Micon 65/13 rotates at 45 rpm and is rated at 65 kW).

The surrounding terrain is essentially flat and characteristic of the Great Plains of the USA. Upwind of the turbine is a meteorological tower instrumented with cup anemometers at hub height (23 meters), rotor top, rotor bottom, and 2 meters from ground level. In addition to the cup anemometers, a wind vane and sonic anemometer are installed at hub height. The anemometry is located approximately 30.7 m upwind of the turbine, or roughly 1.7 rotor diameters in front of the turbine.



**Figure 2. Flapped rotor installed on Micon 65/13M turbine.**

## IV. Suite of Tests

Before the rotor was installed, each blade was characterized with three ground tests: 1) blade pulls in flap and edge with blade cantilevered to test stand, 2) modal test with blade cantilevered to test stand, and 3) modal test with blade suspended in approximate free-free boundary condition. After the rotor was installed on the turbine, the flaps were actuated with various motions to excite structural dynamics while the rotor was parked. These motions consisted of sinusoidal motion at discrete frequencies, sinusoidal motion with logarithmic sweep of frequency, and step motions between 0 degrees flap and  $\pm 5$ , 10, 15, and 20 degrees flap. Finally, these flap actuations were repeated while the rotor was turning and producing power.

This suite of tests was designed to characterize both the non-rotating structural dynamics and the aero-servo-elastic dynamics. The turbine numerical models in FAST<sup>22</sup> and ADAMS<sup>23</sup> are being updated to include the blade properties as calculated from the modal tests and tuned to match the full turbine dynamics observed during operation. This system identification step is crucial for future work on model-based closed-loop control of the flaps.

## V. Time Scales in Aerodynamic Modeling of SMART Rotors

There are several relevant physical time scales, or groups of time scales, involved in wind turbine load control using AALC devices. Understanding these time scales gives insight into the underlying physical processes as well as the ability to assess the validity of various modeling approaches.

The first group of time scales is associated with excitation of the wind turbine aero-elastic system. The excitation inputs to the system include both the turbulent wind input and actuation of the AALC devices. The wind turbulence contains broadband velocity fluctuations, with energy distributed over a continuous range of time scales (and spatial scales). Some of this fluctuation energy occurs at time scales comparable to the wind turbine aero-elastic time scales. This leads to efficient excitation of the wind turbine structure, resulting in dynamic deflections of the blades and tower along with associated fatigue loads. Spatial variations in the mean wind speed due to wind shear, as well as low-frequency turbulent fluctuations that vary in space across the rotor plane, also lead to excitation of the wind turbine at multiples of the rotational frequency.

The device actuation time scale, on the other hand, is associated with the frequency of operation of the AALC device. The achievable range of the device actuation time scale is device-dependent. However, for effective load control the device time scale range needs to include the time scales of important excitation inputs, including the rotational frequency, its harmonics and possibly higher frequency wind events.

The second set of time scales is associated with the structural modes of the wind turbine system; these modes include blade modes (flap-wise, torsional, edge-wise), tower modes, coupled modes, and full system modes. Each mode has a natural frequency with an associated time scale. Typically, the lowest-frequency structural modes are the most important in determining dynamic response and loads. In application of AALC devices, reduction of flap-wise fatigue loads is usually a primary goal, although care must be taken to avoid excessive excitation of torsional and edge-wise modes by the AALC system.

The third set of time scales is associated with aerodynamic phenomena on actively controlled blades. A local blade section flow time scale is associated with the time for a particle to travel the local chord length at the local relative flow velocity, or  $t_f = c/U_{rel}$ . A related aerodynamic time scale is the time for the local two-dimensional flow over a blade section to adjust to a sudden perturbation, such as an instantaneous change in angle of attack or AALC device deployment. This time scale is usually at least several times the local section flow time scale. A third aerodynamic time scale is the wake response time, or the time for the velocity field induced by the rotor trailing vorticity to adjust to a sudden change in blade aerodynamic load distribution. When considering the wake response of a load change on the entire rotor, this time scale is usually much longer than the local section flow time scale, since it is proportional to the ratio of rotor radius to the wind velocity.

Table 1 shows estimates of various time scales for the Sandia 115kW test turbine operating at 55 RPM with a wind speed of 8 m/s. The center of the AALC flapped section is located at 88% of the rotor radius, which is where the local section flow time scale is estimated. The range of AALC device actuation time scales is assumed to include the period of the first two blade flapwise modes, as well as the periods associated with the rotational frequency and two harmonics of the rotational frequency (1P,2P,3P).

**Table 1. Time scales associated with active control of blade fatigue loads for the Sandia 115kW test turbine.**

Process	Time Scale Definition	Time Scale
AALC Device Actuation	Actuation Period	0.03 - 2.0 sec
Response to Rotationally Sampled Wind	1P,2P,3P periods	0.3 - 1.1 sec
Dynamic Structural Response	Period of First Two Blade Flap Modes	0.09 - 0.22 sec
Local Section Flow	Chord / Relative Flow Velocity	0.005 sec
Local Section Flow Adjustment	5-10x Section Flow Time Scale	0.025 - 0.05 sec
Wake Response	Rotor Radius / Wind Speed	1.1 sec

## VI. Results

### A. Time-Average Response to Step Actuation

A sequence of step motions between 0 degrees flap and  $\pm 5, 10, 15,$  and 20 degrees flap was the primary type of flap motion employed to characterize the system response. The duration of each step assumed one of two configurations. First, each step duration was 2.18 seconds which is roughly two rotor revolutions. In this configuration, all these flap positions were cycled through quickly which allowed a rapid characterization of the overall control authority. Second, the duration of each step was extended to 30 seconds so that transient aerodynamic response would reach steady state before another step motion was initiated.

Figure 3 shows the strain response of the most outboard foil strain gage located at 6.75m span to the step sequence with 30-second step duration. Overlaid on the strain response is the flap angle (to facilitate comparison, the strain data has been scaled to be of similar magnitude). The correlation between change in strain and change in flap angle is clearly visible, although turbulent wind conditions have a pronounced effect on strain as well.

Time-averaging of many such responses to the same flap motion reveals the mean flap response hidden beneath the stochastic wind excitation responses. This time-averaging is accomplished by first aligning the signals with a “trigger window” centered on the flap angle signal at a specified trigger level. The following results focus on the 20 degree flap step response and use a trigger level of 19 degrees. The trigger window time is therefore 0.00 seconds when the flap angle passes through 19.0 degrees.

Figure 4 shows the strain signals of 29 individual responses to the 20 degree step motion. Although the random wind excitation produces a wide band of data plotted in gray, consistent structure in the data is evident in the first second after the step transition. The structure is clearly revealed in the average of these 29 responses which is plotted as the thin black line. Figure 5 focuses on the first 1.5 seconds of this mean response. The time delay between the flap motion and strain response is about 0.02 seconds which appears to be consistent with the time scale associated with local section flow adjustment. Although the response is not strictly a “damped free vibration” due to the presence of both constant and random wind excitation, application of the theory for damped free vibration provides some insight into the response. First, the frequency of vibration is calculated from the time between peaks to be 4.17 Hz which matches the first flapwise blade bending mode. Second, the damping ratio  $\zeta$  for damped free vibration can be calculated from the logarithmic decrement<sup>24</sup>, here denoted by  $\delta$  in Eq. (1). The logarithmic decrement is simply the natural logarithm of the ratio  $u_i / u_{i+1}$  of two successive peak values. If  $\zeta$  is small such that the denominator in the right hand expression of Eq. (1) is approximately 1, then the damping ratio can be easily

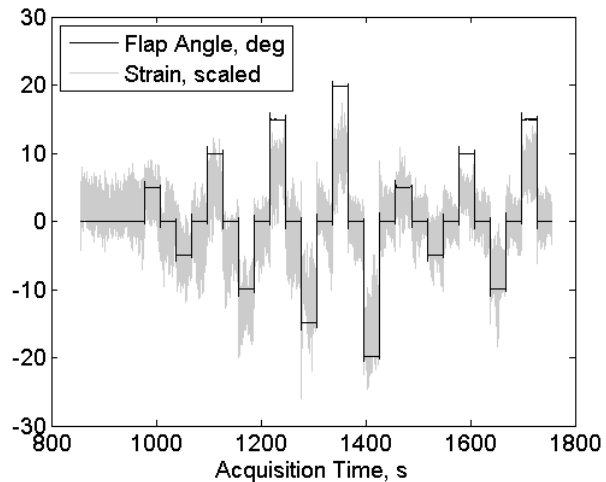


**Figure 3. Strain response to flap step sequence (6.75m span).**

calculated from Eq. (2). Using these equations, a damping ratio on the order of 1% to 3% was calculated from the peaks seen in Figure 5 using the information contained in Table 2.

$$\delta = \ln \frac{u_i}{u_{i+1}} = \frac{2\pi\zeta}{\sqrt{1-\zeta^2}} \quad (1)$$

$$\zeta \approx \frac{\delta}{2\pi} \quad (2)$$

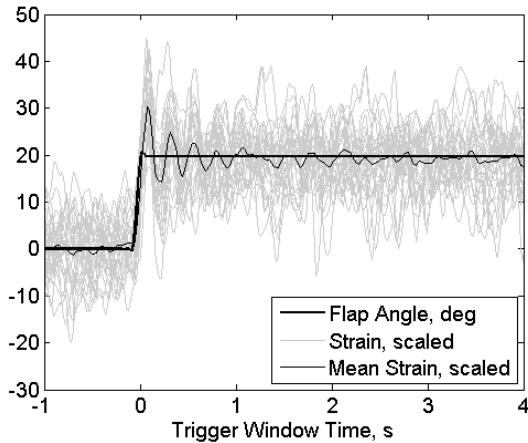


Figure 4. Time-averaged strain response to 20 degree flap step.

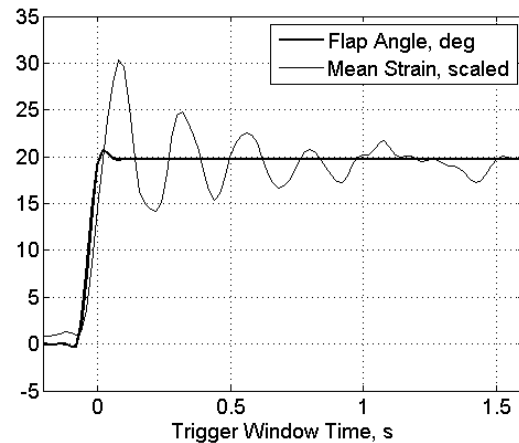


Figure 5. Detail of strain oscillations in step response.

Table 2. Damped free vibration parameters from strain response.

Peak	Maximum	Time, s	Peaks	Log Decrement	Damping Ratio	Time Difference, s	$1 / \Delta T, s^{-1}$
$u_1$	30.38	0.0799	$u_2-u_1$	0.202	0.032	0.2396	4.17
$u_2$	24.83	0.3195	$u_3-u_2$	0.097	0.015	0.2397	4.17
$u_3$	22.54	0.5592	$u_4-u_3$	0.080	0.013	0.2396	4.17
$u_4$	20.81	0.7988					

Using the same time-averaging procedure, the mean response of generator power seen in Figure 6 reveals a subtle jump in power output approximately 0.22-0.26 seconds after the flap step motion. It may be a coincidence, but this delay matches the period of blade flapwise motion. In addition, the maximum power after the step occurs only 0.06 seconds after the blade strain oscillation reaches the first minimum (see Figure 5 at 0.22 seconds). The upwind swing of the blade against the flow appears to be the cause of the momentary jump in power. Future work will test this hypothesis using an aero-elastic code with a dynamic wake model.

Looking at the individual power output signals plotted in gray in Figure 6, the jump is visible in many of the waveforms, however, the amount of variation between signals suggests that attempting to draw any additional conclusions from the mean response may be asking too much. It is likely that more than 29 response signals need to be averaged and/or the wind speed needs to be taken into account in order to accurately identify other repeatable dynamics being exhibited here.

Signals from the inertial measurement unit (IMU) mounted on the nacelle bedplate were also examined using the time-averaging approach. Plotted in Figure 7, the y-component which senses side-to-side tower motion shows that a substantial ringing is induced at tower top approximately 0.05 seconds after the flap step motion.

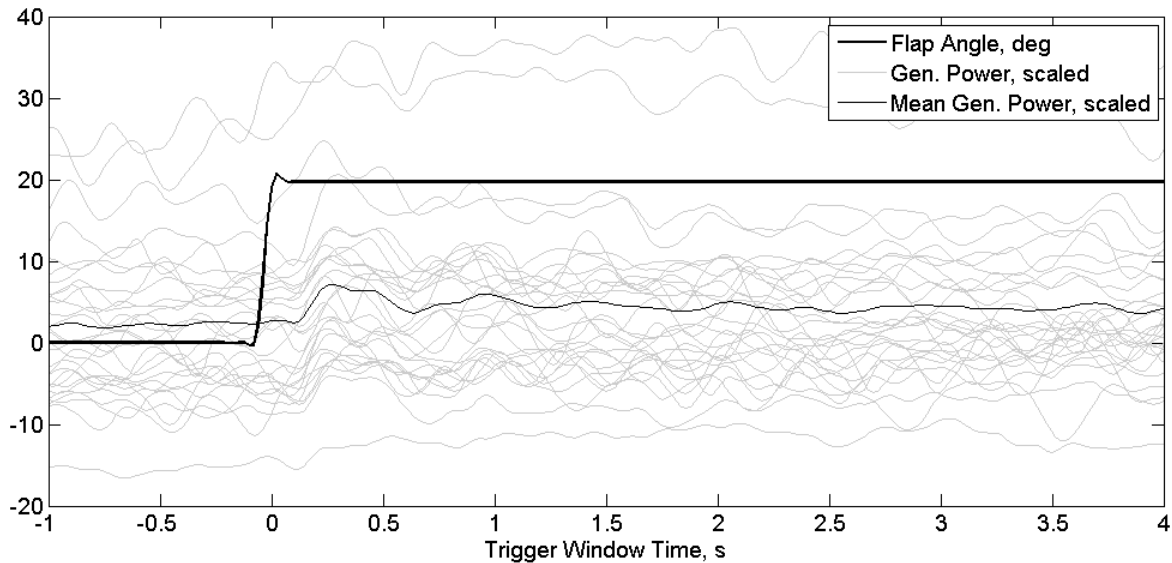


Figure 6. Time-averaged generator power response to 20 degree flap step.

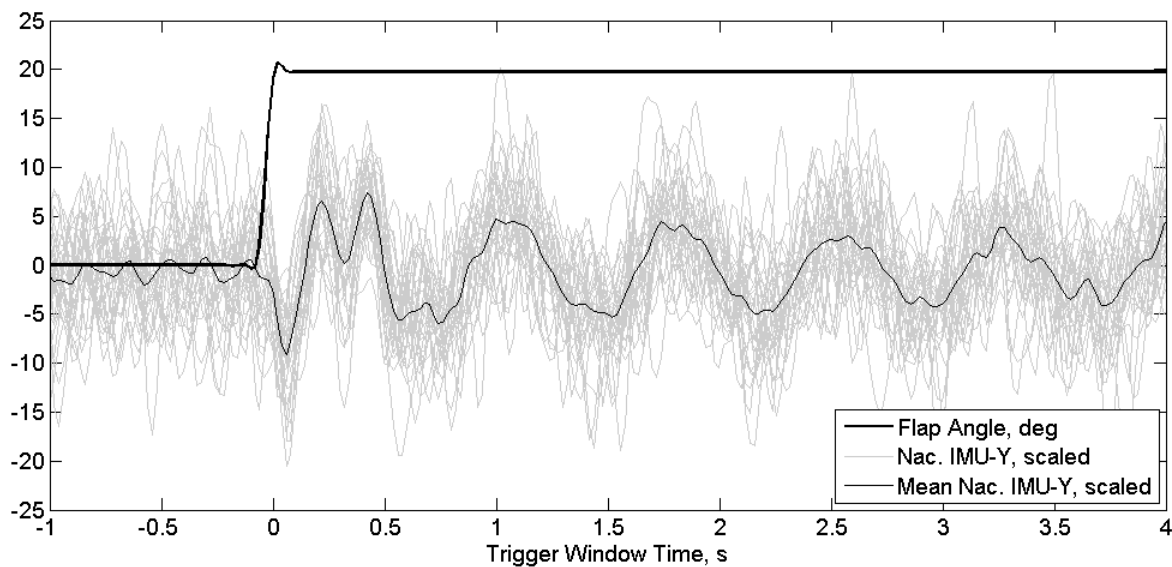
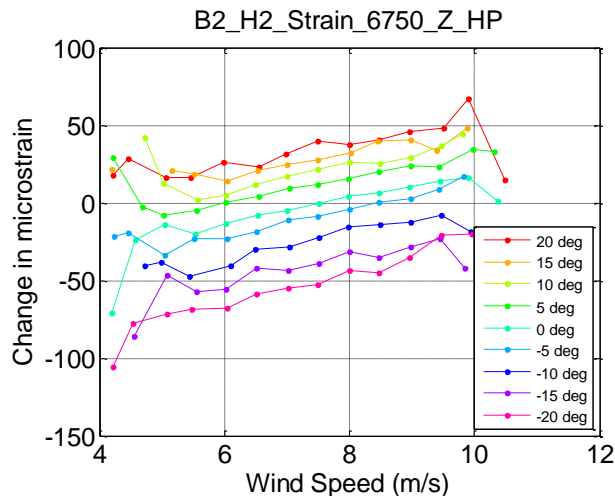


Figure 7. Time-averaged response of y-component of nacelle IMU to 20 degree flap step.

## B. Average Response Binned by Wind Speed and Flap Angle

The curves in Figure 8 are produced by binning the data according to wind speed and then averaging the strain response for each flap position. Similar results are obtained for the other three strain gage locations. The overall character of these curves matches the expectations from simulation. The control authority on the positive flap angle side is somewhat less than that on the negative flap angle side likely due to the initiation of stall with high positive flap angles.



**Figure 8. Average strain response curves as a function of wind speed and flap angle (6750 mm span).**

### C. Sine Sweep, Parked Rotor

Sinusoidal flap motion with logarithmic sweep of frequency was used to provide a driving force over a range of frequencies. With the rotor parked, the inertia of the flap generated the controlled frequency input while the ambient inflow created a small random buffeting input on the flat of the blade. Figure 9 is the spectrogram of the flapwise acceleration during a test which swept over the frequency range 0.1 to 10 Hz in 500 seconds. The red curve is the logarithmic frequency input and the vertical lines are structural resonance frequencies. The other curves following the shape of the red curve are harmonics of the main input frequency. Broadband frequency input up to about 15 Hz is visible in the background due to the random wind buffeting. The PSD of this same test for all three blades given in Figure 10 shows a more refined view of the individual frequency response peaks.

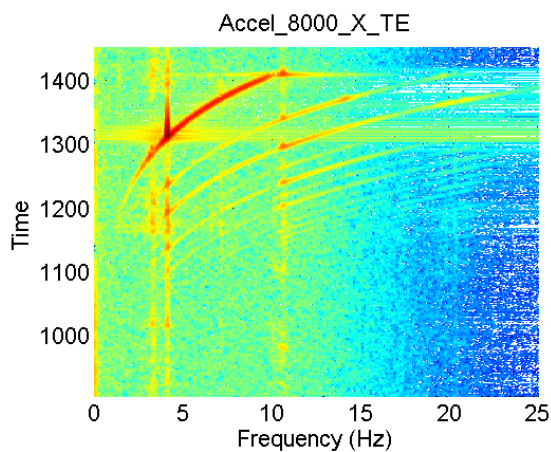


**Figure 9. Parked rotor spectrogram (waterfall plot) of flapwise acceleration at 8000 mm span with logarithmic sine sweep.**

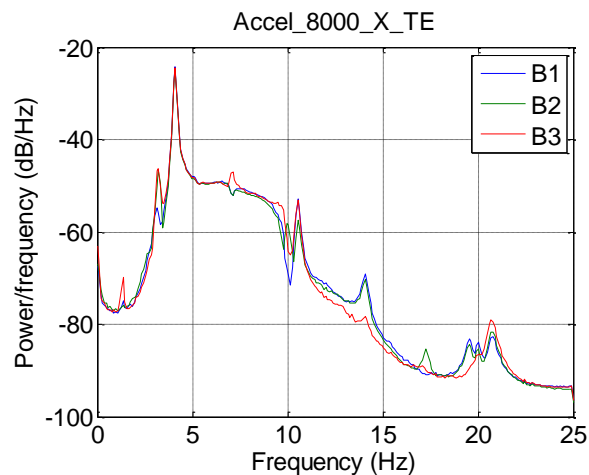


**Figure 10. Parked rotor PSD of flapwise acceleration at 8000 mm span with logarithmic sine sweep.**

### D. Sine Sweep, Power Production

Similar sinusoidal flap motion with logarithmic sweep of frequency was applied while the rotor was turning at 55 rpm and the generator was producing power. As seen in Figure 11 and Figure 12, the primary structural resonance is present but the peak is much wider which indicates increased damping resulting from the addition of aerodynamic damping forces. An upshift in this peak's frequency is observed from 4.1 Hz in the non-rotating test to

4.4 Hz in the power production test. This upshift is likely due to rotational stiffening of the blades. The spectrogram has a number of vertical lines at regular intervals which are harmonics of the rotor frequency (1P, 2P, etc.).

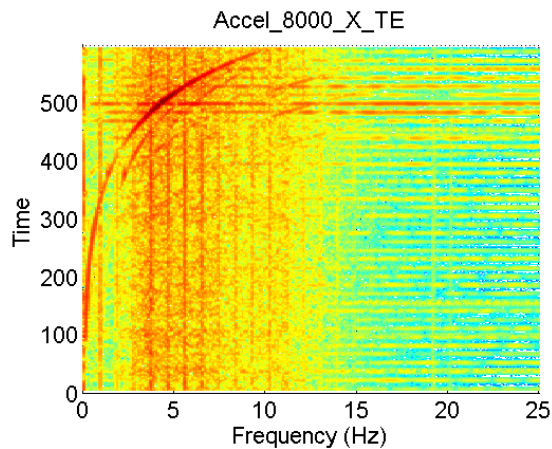


**Figure 11. Power production spectrogram (waterfall plot) of flapwise acceleration at 8000 mm span with logarithmic sine sweep.**

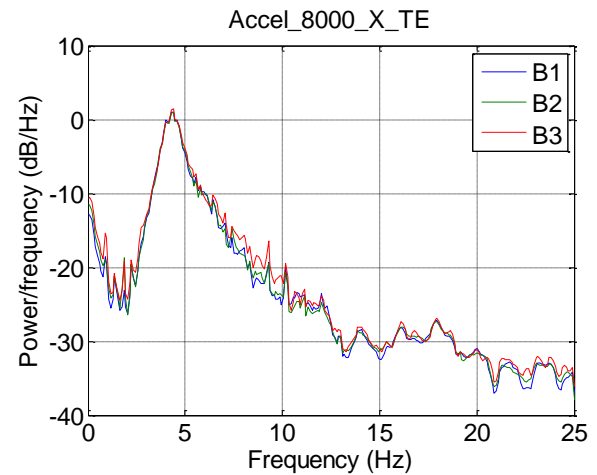


**Figure 12. Parked rotor PSD of flapwise acceleration at 8000 mm span with logarithmic sine sweep.**

Hub mounted video cameras pointed toward the blade tips were used to capture the tip motion during some of the test runs, including one power production sine sweep test. Figure 13 is a sequence of still images over one flap cycle when the blade was excited at the main resonance frequency. The blade tip is initially downwind or to the left (frame 1) when the flaps begin moving toward the lower pressure surface. The reduced lift results in tip movement upwind or to the right (frame 5). As the flaps move back to their initial position, the blade tip also moves back to the initial position (frame 9).



**Figure 13. This sequence of camera stills of a sinusoidal flap motion shows the blade tip moving from a downwind position (1) to an upwind position (5) and back to the downwind position (9) during one flap cycle**

## VII. Conclusion & Future Work

The Sandia SMART rotor field test has concluded and initial analysis clearly shows that the trailing-edge flaps directly affect blade strain and tip motion. The full suite of test data is currently being examined and the aero-servo-elastic models will be updated and evaluated regarding the degree to which they capture the important dynamics

which have been described in this paper. Future work will likely involve development and implementation of improved models to accurately capture the local flow and wake effects that have been observed thus far.

### Acknowledgments

The authors gratefully acknowledge the contributions of USDA-ARS staff provided throughout the field testing phase of this project, in particular Adam Holman (WTAMU) and Byron Neal. The authors also gratefully acknowledge the following Sandia staff for their contributions: Dale Berg, Wesley Johnson, Mark Rumsey, Jon White, Bruce LeBlanc, Gary Fischer, Mike Kelly, Josh Paquette, and David Wilson.

### References

- <sup>1</sup>Barlas, T.K. and van Kuik, G.A.M., Review of state of the art in smart rotor control research for wind turbines, *Progress in Aerospace Science* (2009), doi:10.1016/j.paerosci.2009.08.002
- <sup>2</sup>van Wingerden, J-W., Hulschapp, A.W., Barlas, T., Marrant, B, van Kuik, G.A.M., Molenaar, D-P, and Verhaegen, M., On the Proof of Concept of a ‘Smart’ Wind Turbine Rotor Blade for Load Alleviation, *Wind Energy*, 2008; 11:265-80.
- <sup>3</sup>Barlas, T., van Wingerden, J-W, Hulschapp, A, and van Kuik, G, “Closed-loop Control Wind Tunnel Tests on an Adaptive Wind Turbine Blade for Load Reduction,” *Proceedings of the 46th AIAA/ASME*, Reno, NV, USA, 2008.
- <sup>4</sup>Troldborg, N., Computational study of the Risø B1-18 airfoil with a hinged flap providing variable trailing edge geometry. *Wind Engineering* 2005, 29:89-113.
- <sup>5</sup>Buhl, T., Gaunaa, M., and Bak, C., “Load reduction potential using airfoils with variable trailing edge geometry,” *Proceedings of the 43th AIAA/ASME*, Reno, NV, USA, 2005.
- <sup>6</sup>Buhl, T., Gaunaa, M., and Bak, C., Potential load reduction using airfoils with variable trailing edge geometry. *Solar Energy Engineering* 2005, 127:503-16.
- <sup>7</sup>Andersen, P. B., Gaunaa, M., Bak, C., and Buhl, T., “Load alleviation on wind turbine blades using variable airfoil geometry,” *Proceedings of the EWEC 2006*, Athens, Greece.
- <sup>8</sup>Andersen, P. B., Gaunaa, M., Bak, C., and Buhl, T., “Wind tunnel test on wind turbine airfoil with adaptive trailing edge geometry,” *Proceedings of the 45th AIAA/ASME*, Reno, NV, USA, 2007.
- <sup>9</sup>Buhl, T., “Stability Limits for a Full Wind Turbine Equipped with Trailing Edge Systems,” European Wind Energy Conference, Marseille, France, 16-19 March, 2009.
- <sup>10</sup>Anderson, P.B., “Load Reduction Using Pressure Difference on Airfoil for Control of Trailing Edge Flaps,” European Wind Energy Conference, Marseille, France, 16-19 March, 2009.
- <sup>11</sup>Wilson, D.G., Berg, D.E., Barone, M.F., Berg, J.C., Resor, B.R., and Lobitz, D.W., “Active Aerodynamic Blade Control Design for Load Reduction on Large Wind Turbines” European Wind Energy Conference, Marseille, France, 26-19 March, 2009.
- <sup>12</sup>Berg, D.E., Wilson, D.G., Barone, M.F., Berg, J.C., Resor, B.R., Paquette, J.A., and Zayas, J.R., “The Impact of Active Aerodynamic Load Control on Fatigue and Energy Capture at Low Wind Speed Sites,” European Wind Energy Conference, Marseille, France, 16-19 March, 2009.
- <sup>13</sup>Berg, D.E., Wilson, D.G., Resor, B.R., Barone, M.F., Berg, J.C., Kota, S. and Ervin, G., “Active Aerodynamic Blade Load Control Impacts on Utility-Scale Wind Turbines,” WINDPOWER 2009, Chicago, Illinois, 5-7 May, 2009.
- <sup>14</sup>Wilson, Berg, D.E., D.G., Resor, B.R., Barone, M.F., and Berg, J.C., “Combined Individual Pitch Control and Active Aerodynamic Load Controller Investigation for the 5MW UpWind Turbine, WINDPOWER 2009, Chicago, Illinois, 5-7 May, 2009.
- <sup>15</sup>Resor, B., Wilson, D., Berg, D., Berg, J., Barlas, T., and van Kuik, G., “The Impact of Higher Fidelity Models on Active Aerodynamic Load Control Fatigue Damage Reduction,” *Proceedings of the 48th AIAA Aerospace Sciences Meeting*, Orlando, FL, January 4-7, 2010.
- <sup>16</sup>Wilson, D.G., Resor, B.R., Berg, D.E., Barlas, T.K., and van Kuik, G.A.M., “Active Aerodynamic Blade Distributed Flap Control Design Procedure for Load Reduction on the UpWind 5MW Wind Turbine,” *Proceedings of the 48th AIAA Aerospace Sciences Meeting*, Orlando, FL, January 4-7, 2010.
- <sup>17</sup>Berg, D. E., Wilson, D., Resor, B., Berg, J., Barlas, T., Crowther, A. and Halse, C., “System ID Modern Control Algorithms for Active Aerodynamic Load Control and Impact on Gearbox Loading,” *The Science of Making Torque from Wind*, 2010.
- <sup>18</sup>Chow, R., and van Dam, C.P., “Unsteady Computational Investigations of Deploying Load Control Microtabs,” *Journal of Aircraft*, Vol. 43, No. 5, Sept-Oct 2006, pp. 1458-1469.
- <sup>19</sup>Berg, D.E., Zayas, J.R., Lobitz, D.W., van Dam, C.P., Chow, R., and Baker, J.P. “Active Aerodynamic Load Control of Wind Turbine Blades,” *Proceedings of the 5<sup>th</sup> Joint ASME/JSME Fluids Engineering Conference*, San Diego, CA, July 2007, FEDSM2007-37604.
- <sup>20</sup>Berg, J., Berg, D., White, J., “Fabrication, Integration and Initial Testing of a SMART Rotor,” *Proceedings of the 50th AIAA Aerospace Sciences Meeting*, Nashville, Tennessee, 2012
- <sup>21</sup>Berg, D., Berg, J., Wilson, D., White, J., Resor, B., Rumsey, M., “Design, Fabrication, Assembly and Initial Testing of a SMART Rotor,” *Proceedings of the 49th AIAA Aerospace Sciences Meeting*, Orlando, Florida, 2011
- <sup>22</sup>NWTC Computer-Aided Engineering Tools (FAST by Jason Jonkman, Ph.D.).  
<http://wind.nrel.gov/designcodes/simulators/fast/>. Last modified 3-December-2012.

<sup>23</sup>MSC Software. Adams: Multibody Dynamics Simulation. <http://www.mscsoftware.com/Products/CAE-Tools/Adams.aspx>

<sup>24</sup>Chopra, A.K., *Dynamics of Structures*, 2<sup>nd</sup> Edition, Prentice Hall, Upper Saddle River, New Jersey, 2001